Journal Pre-proof

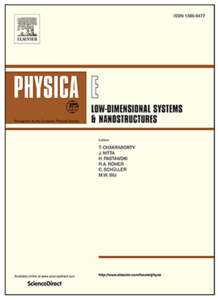

Weak antilocalization to weak localization transition in Bi_2Se_3 films on graphene

N.P. Stepina, V.A. Golyashov, A.V. Nenashev, O.E. Tereshchenko, K.A. Kokh, V.V. Kirienko, E.S. Koptev, M.G. Rybin, E.D. Obraztsova, I.V. Antonova

PII: S1386-9477(21)00337-4
DOI: https://doi.org/10.1016/j.physe.2021.114969
Reference: PHYSE 114969

To appear in: *Physica E: Low-dimensional Systems and Nanostructures*

Received date : 26 April 2021
Revised date : 27 August 2021
Accepted date : 7 September 2021

Please cite this article as: N.P. Stepina, V.A. Golyashov, A.V. Nenashev et al., Weak antilocalization to weak localization transition in Bi_2Se_3 films on graphene, *Physica E: Low-dimensional Systems and Nanostructures* (2021), doi: https://doi.org/10.1016/j.physe.2021.114969.

Weak antilocalization to weak localization transition in Bi_2Se_3 films on graphene

N. P. Stepina[a], V. A. Golyashov[a], A. V. Nenashev[a], O. E. Tereshchenko[a], K. A. Kokh[c], V. V. Kirienko[a], E. S. Koptev[a,b], M. G. Rybin[d], E. D. Obraztsova[d] and I. V. Antonova[a]

[a] *Rzhanov Institute of Semiconductor Physics SB RAS, Novosibirsk, 630090, Russia*
[b] *Novosibirsk State Technical University, Novosibirsk, 630073, NovosibirskRussia*
[c] *Sobolev Institute of geology and mineralogy SB RAS, Novosibirsk 630090, Russia*
[d] *Prokhorov General Physics Institute, RAS, Moscow, 119991, Russia*

ABSTRACT

Magneto-transport properties were studied on thin films of a 3D topological insulator (TI) Bi_2Se_3 grown on graphene (Gr) by physical vapor deposition. It was shown that the main contribution to the conductance is from the bulk states, whereas magnetoresistance is determined by both surface and bulk channels. The input of the charge transport over the surface states in the $Si/SiO_2/Gr/Bi_2Se_3$ structure reveals itself in the weak antilocalization effect. The transition from a weak antilocalization to a weak localization is observed with decreasing the film thickness. The band bending on both interfaces makes it possible to explain the contribution to a weak antilocalization from different surfaces at different TI film thicknesses.

1. Introduction

Three-dimensional topological insulators (TIs), along with the bulk conductivity, which is determined by the band gap and the doping level of the material, has conducting spin-split surface states as a consequence of strong spin-orbit coupling [1, 2]. Being protected by the time reversal symmetry, these surface states consist of an odd number of Dirac cones, with the spin direction being orthogonal to the wave vector and uniquely related to it. The Berry phase π for the carriers on topological surface states determines the weak antilocalization (WAL) appearance [2]. WAL is observed in a variety of different films with large spin orbit interaction [3, 4]. In TIs both the bulk and surface states contribute to the coherent transport, and, in both cases, they are expected to exhibit WAL. However, experimentally, the logarithmic suppression of conductivity with decreasing temperature, typical for the weak localization (WL) regime, is most often observed in TIs. This phenomenon is known as the transport paradox [5] in TIs. Despite the dominance of bulk conductivity, in topological insulators, the WAL appears to be weakly related to bulk states. As a result, it was suggested [5] that the experimentally observed WAL can be a collective effect of WAL related to the surface channels and WL of a bulk channel. The electron-electron interaction [6], as well as the surface states mixing of the upper and lower boundaries [7], was proposed as an explanation of the observed WL.

One of the most intensively investigated 3D TIs are narrow-gap semiconductor compounds of V-VI groups [8, 9, 10, 11]. The presence of topological surface states with a linear dispersion law in various Bi-Sb-Se-Te films (Bi_2Te_3, Bi_2Se_3, $BiSbTeSe_2$) was experimentally confirmed using the methods of photoemission spectroscopy with angular resolution and scanning tunneling spectroscopy [12, 13, 14].

The main problem in the transport study in two-component compounds (Bi_2Se_3 type) is the domination of the bulk conductivity over that for surface states. To reduce the bulk contribution, two approaches are typically used, the reduction of the film thickness and compensation with various impurities, such as calcium [15]. Another possibility is to change the composition of the material, namely to use ternary [16] or quaternary compounds [17, 18]. Thus, by choosing a three-component material, in which the bulk conductivity was significantly reduced, the authors of [19] could observe the contribution of surface states in the magnetoresistance (MR) of ultrathin $(Bi_{0.57}Sb_{0.43})_2Se_3$ films.

It is worth to note that the quantum corrections to the conductivity $\Delta\sigma$ do not depend on which channel dominates in conductivity σ itself. Thus even if the bulk conductivity is much higher than the surface one, the quantum corrections $\Delta\sigma$ from the surface channels may not be masked by the contribution of the bulk. Which channel prevails in $\Delta\sigma$ is defined by the corresponding values of the characteristic times, phase coherence time τ_ϕ, spin relaxation time τ_s and mean free time τ_p.

One of the feasible ways to engineer the topological surface states is to use the proximity effect in TI/non-TI heterostructures. It is theoretically predicted [20, 21, 22] that the combination of two materials, a graphene (Gr)-like one and a TI, promotes the proximity effects which can significantly change the properties of van der Waals heterostructures, up to the creation of a 2D topological phase and the appearance of a spin quantum Hall effect in graphene. In [23] the authors use *ab initio* simulations and tight-binding models to determine the precise spin texture of electronic states in graphene interfaced with a Bi_2Se_3 TI. Their calculations predict the emergence of a giant spin lifetime anisotropy in the graphene layer, which should be a measurable hallmark

nstepina@mail.ru (N. P. Stepina)
ORCID(s):

of spin transport in Gr/TI heterostructures and suggest novel types of spin devices.

The authors [24] claimed that the strain and band bending on the TI/graphene interface result in the localization of surface states on each top and bottom layer and suppress the overlap of two surface states. It was shown [25] that the renormalization of hybrid graphene bands can leave the spin texture of TI surface states unchanged even in the presence of defects at the interface. The experimental study demonstrates [26] that the integration of two-dimensional graphene with a three-dimensional TI in van der Waals heterostructures takes the advantage of their remarkable spintronic properties and produces proximity-induced spin-charge conversion phenomena. However, practically in most cases, they used exfoliated Gr [27, 28] or an exfoliated TI [26] and, correspondingly, the only μm-sized structures were possible to investigate.

This work is devoted to the study of the magnetotransport properties of Bi_2Se_3 thin films grown on graphene. We use large area graphene grown by chemical vapor deposition (CVD). The contribution of the charge transport over the surface states in Si/SiO_2/Gr/Bi_2Se_3 heterostructures reveals itself in the WAL effect in MR. The good quality of the graphene/TI interface gives the possibility to obtain the input to the MR from this surface even in mm-sized structures. The band bending on both interfaces makes it possible to obtain the contribution from different surfaces at different TI film thicknesses.

2. Samples and experiment

Bi_2Se_3 films were grown on the Si/SiO_2/Gr substrate. The graphene samples were provided by the company "RusGraphene". Graphene was synthesized using the method of chemical deposition in the gas phase, implemented in a cold wall installation and resistive heating of a copper foil. The methane introduction into the chamber at the concentration of 1% and the temperature of 850°C for 5 minutes leads to a growth of graphene. The transfer of graphene from the copper foil to a 300 nm SiO_2/Si substrate was carried out by the standard technology using PMMA as a supporting polymer.

Bi_2Se_3 films were grown by means of the physical vapor deposition at a source temperature of about 500°C. The reactor consists of the quartz glass ampoule that was placed with a sealed end in a horizontal heating furnace. The opposite end was kept at room temperature and was connected to the forevacuum pump. There were two boats inside the reactor. The first one was in the region with a high temperature containing the charge of a Bi_2Se_3 single crystal fragment. The second boat with substrates was located in the temperature gradient region.

To reveal the effect of graphene on the transport properties of the structure, we additionally prepared Bi_2Se_3 films grown on mica. Before the loading into the reactor the surface layer of mica was removed by scotch.

According to atomic force microscopy, the total thickness of Bi_2Se_3 films grown on graphene was about 20, 30, and 50 nm in the samples studied in this work. We named these samples as 1, 2 and 3 in the order of thickness increase. The detailed structural and electro-physical properties of these samples were described in our previous paper [29]. Contacts for transport measurements were created by sputtering indium with a subsequent soldering of silver wires using indium solder. The magnetoresistance and temperature dependences of conductivity were measured in a transport helium Dewar vessel in a magnetic field up to 4 T with the possibility of turning the magnetic field.

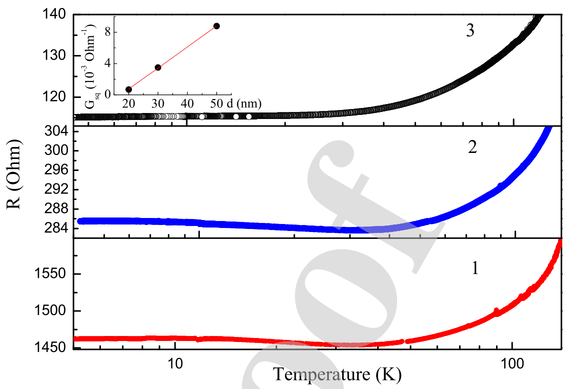

Figure 1: Temperature dependence of resistance for samples with different Bi_2Se_3 film thicknesses d. Inset – conductivity *versus* d at T=4.2 K.

3. Experimental data

In Fig. 1 are the temperature dependences of the resistance of Bi_2Se_3 films grown on graphene. At high temperatures all films exhibit an increase in the resistance with increasing the temperature that typically explained by the enhancement of phonon scattering. For film 3, the metallic behavior of conductivity is observed for the entire temperature range, whereas, for films 2 and 1, the resistance begins to increase with decreasing the temperature below 30 K. Such increase in the resistance is most likely determined by the quantum corrections to the conductivity associated with the electron-electron interaction or weak localization. The inset to Fig. 1 demonstrates the linear dependence of sheet conductivities measured at T=4.2 K on the film thickness indicating that, for all samples under study, the conductivity is mainly determined by bulk states.

When a perpendicular to the film magnetic field is applied, samples 2 and 3 show the negative magnetoconductance (MC) with a cusplike maximum at $B = 0$ (Fig. 2). Such behavior is typical of the WAL effect expected for the transport over topological surface states in three-dimensional topological insulators. Due to the nonzero Berry phase in zero magnetic field, a positive quantum correction to the conductivity arises, and it sharply decreases with an increase of the magnetic field. The WAL value becomes smaller for the sample 2 and, in larger magnetic fields, it goes to the positive MC, typical of a quantum correction to the conductivity associated with the WL. For the thinnest sample 1, instead of a negative MC, a positive MC is observed even in the lowest

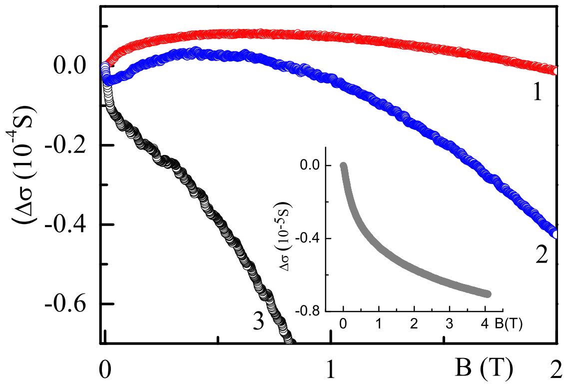

Figure 2: Magnetoconductance $\Delta\sigma(B) = \sigma(B) - \sigma(0)$ of the samples under study in the magnetic field perpendicular to the sample plane, T=4.2 K. Inset – MC for the film grown on mica with the film thickness similar to that for sample 3.

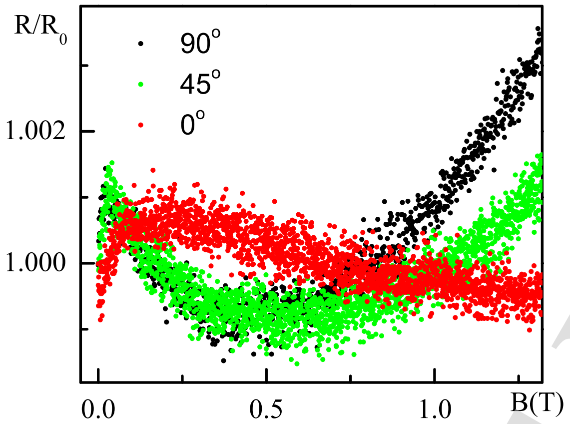

Figure 3: Magnetoresistance of the film 2 at different angles of magnetic field to the sample plane, T=4.2 K. 0° – magnetic field parallel to the sample plane.

magnetic fields.

The orbital nature of the WL is clearly indicated (Fig. 3) by the broadening of the negative MR at the sample rotation from a magnetic field, perpendicular to the sample plane, to a parallel field (θ=0°). The presence of a residual final MR in the field close to the parallel one can be associated with the nonuniform thickness of the Bi_2Se_3 film as a consequence of the partially inclined upper surface, on which the local electron transport can have a finite angle to the magnetic field.

To reveal the influence of graphene on the TI transport properties, the MC of the Bi_2Se_3 film grown on mica with the film thickness similar to that for sample 3 was also measured. The result for the magnetic field oriented perpendicular to the sample plane is shown in the inset to Fig. 2. One can see that the behavior is quite different from that for the samples grown on graphene: one order smaller change in $\Delta\sigma$ and wider range of WAL (up to B=4 T) is observed. A larger width of the WAL curve reflects a smaller phase coherent length L_i.

In order to obtain the quantitative characteristics of the experimental data, the conductivity of the films in a mag-

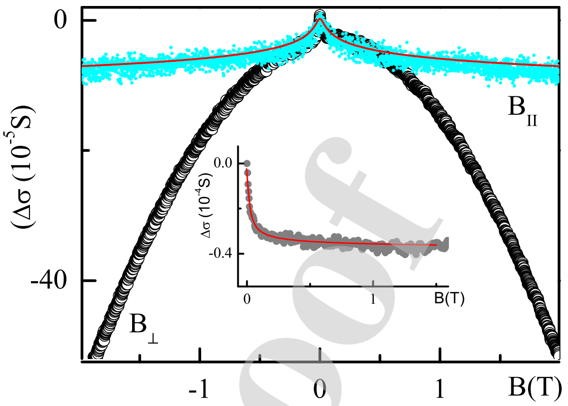

Figure 4: Magnetoconductance $\Delta\sigma(B) = \sigma(B) - \sigma(0)$ of sample 3 in parallel ($B_{||}$) and perpendicular ($B_\perp$) magnetic field. T = 4.2 K. Inset – $\Delta\sigma(B)$ for $B_\perp$ after subtracting the quadratic Lorentzian contribution. $\alpha_{WL} \sim 1$, $\alpha_{WAL} \sim -1$, $L_{WL} \sim 0.14\mu$m, $L_{WAL} \sim 0.46\mu$m, $\beta_{WL} \sim 0.04$, $\beta_{WAL} \sim 0.2$.

netic field $\Delta\sigma(B) = \sigma(B) - \sigma(0)$ was analyzed using two Hikami-Larkin-Nagaoki functions [30], which describe the suppression of WL and WAL in a magnetic field (1):

$$\Delta\sigma(B) = \sum_{i=1}^{2} \alpha_i \frac{e^2}{\pi h} \left[\Psi\left(\frac{\hbar}{4eBL_i^2} + \frac{1}{2} \right) - \ln\left(\frac{\hbar}{4eBL_i^2} \right) \right] \tag{1}$$

The formula has 2 terms: one for WL and the other for WAL, characterized by the parameter α. Here α is a constant of the order of 1 for the WL and –1/2 for the WAL when considering single conduction channel, $\Psi(x)$ is the digamma function.

In the perpendicular magnetic field, sample 3, along with WAL, shows a parabolic B-field dependence of MC. This semiclassical B^2 dependence results from the Lorentz deflection of carriers [32]. According to the Kohler rule [31], $R(B)/R(B = 0) \sim 1 + (\mu B)^2$, the film mobility μ is estimated to be 760 cm^{2}V^{-1}s^{-1} for sample 3 and 604 cm^{2}V^{-1}s^{-1} for sample 2. By substracting the background parabola from MC, we obtain the WAL-induced quantum corrections to MC, $\Delta\sigma(B) = \sigma(B) - \sigma(0)$.

The MC in the perpendicular and parallel field for sample 3 is shown in the Fig. 4. The inset to Fig. 4 depicts the MC in the perpendicular field after substracting the quadratic Lorentzian contribution. The line in the inset is the approximation of the experimental data by formula (1). As a result of the approximation, constants α_i and L_i were obtained: $\alpha_{WL} \sim 1$ and $\alpha_{WAL} \sim -1$ for the case of WL and WAL, respectively; $L_{WL} \sim 0.14\mu$m, $L_{WAL} \sim 0.46\mu$m. The fact that $\alpha_{WAL} \sim -1$ indicates that the contribution to the WAL is made by 2 channels, which are apparently determined by the upper (Air/TI) and lower (Gr/TI) boundaries of the topological insulator. A similar approximation for the film 2 $\alpha_{WL} \sim 1$, $\alpha_{WAL} \sim -1/2$, $L_{WL} \sim 0.16\mu$m, $L_{WAL} \sim 0.51\mu$m. The decrease of the α_{WAL} down to -1/2 indicates on a single channel contribution to the WAL effect. For sample 1, the MR is described with the only WL taken into account.

The analysis of the MC for mica film shows the only WAL contribution with a small value of $\alpha_{WAL} \sim -0.45$ and $L_{WAL} \sim 0.1\mu$m.

4. Discussion

The $\alpha_{WAL} \sim -1$ value is rarely observed in 3D TI films. In the most papers the authors obtain $\alpha_{WAL} \sim -1/2$ [7, 33]. Chen et al. [7] and He et al. [34] claimed that the bottom surface would not contribute much to MC because of the short phase coherence length due to defects. The characteristic feature of TI films grown on graphene is the structurally perfect interface [35, 24] without typical growth defects. Thus, in the thick sample 3, we can see the contribution from two boundaries due to the improved properties of the bottom interface. The sample on mica with approximately the same thickness is characterized by one channel WAL confirmed that the films grown on graphene have better bottom interface than that for the mica case. A three times smaller L_{WAL} for the on-mica grown film, as compared with L_{WAL} for film grown on graphene, is also characterized by the better structure of on-graphene grown films. A decrease of α_{WAL} to $\sim -1/2$ in thinner films indicates the dissapearance of the one channel input to WAL or shows the onset of two surface hybridization.

The transition from WAL to WL was observed in TIs in many experiments, in particular, upon doping with magnetic impurities [36, 37], as well as when decreasing the TI film thickness. In the compound $(Bi_{0.57}Sb_{0.43})_2Se_3$ [19] such a transition occurred when the film thickness changed from 6 to 4-5 quintilayers (QLs). The authors explained the WAL peak disappearance by the hybridization of surface states on the upper and lower surfaces, the corresponding opening of a gap in thin film electronic spectrum and the transformation of the Dirac cone into two bands with nonzero effective masses, as was shown by the ARPES method [38, 39, 40, 41]. The opening of the gap leads to a change in the Berry phase [42]

$$\phi_B = \pi \left(1 - \frac{\Delta}{2E_f}\right) \tag{2}$$

from π to 0 and, accordingly, to a transition from WAL to WL. Here Δ is the gap, E_f is the Fermi energy measured from the Dirac point.

At first sight, the MC behavior, in our case, is very similar to that obtained by the authors of [19] for the ultrathin TI films. However, the thickness of our structures under study is far from 4-6 QLs. We interpreted a different α_{WAL} value and the transition from WAL to WL for the films with different thickness d as an effect of band bending on the TI/Gr and TI/Air interfaces. The authors of [43] showed with ARPES that the conduction band edge and the Dirac point of the cleaved Bi_2Se_3 film shifts gradually downwards after three hours in vacuum due to defect-induced band bending near

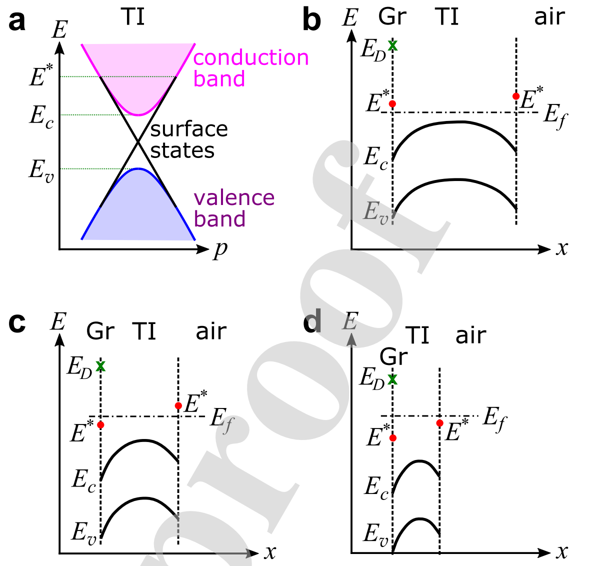

Figure 5: a – Schematic of the energy to wave-vector dependence for Bi_2Se_3 film. Sketches of band diagrams for Gr/Bi_2Se_3/air structure with the thicknesses of TI layer: b – 50 nm, c – 30 nm, d – 20 nm. E_c and E_v are volume band edges in bulk TI, E^* is the upper boundary of the surface-state energy on the TI boundary, E_D is the Dirac point in graphene, and E_f is the Fermi level.

the surface. In our case, it is important to take into account also the second interface. As the Dirac point of graphene film is higher than the TI conductivity band edge E_c [24], electrons from graphene move to the TI, thus, creating the accumulation region. With a decrease of the film thickness, the 3D electron concentration increases and E_c goes down, with respect to the Fermi level E_f.

The order of the band bending magnitude was estimated by solving the Poisson equation with the following parameters: bulk dielectric constant ϵ=113 [43], an electron effective mass $m^* = 0.1m_e$, bulk donor concentration $N_d = 10^{18}$ cm^{-3}; the band offset between the Dirac point in graphene and the conduction band edge in TI was taken as 0.35 eV. For the simplicity we do not take into account the quantum confinenment. The TI film is proposed to be homogeneously n-type dopped. E_f position is determined by the condition that the total charge of holes in graphene, electrons in TI, surface states at the top surface and ionized impurities in the bulk is equal to zero. For the 50 nm thick film the band bending on the TI/Gr boundary was found to be about 0.07 eV, and to decrease down to 0.04 for 20 nm thick film.

A qualitative band diagram for the Bi_2Se_3/Gr structure with three different film thicknesses is demonstrated in Fig. 5.

Fig. 5, a is a sketch of the TI band structure with topological surface states. These surface states cover the range of energies up to some energy E^* which is higher than E_c. For simplicity, we suggest that the topological surface states contribute to the conductance as long as E_f is lower than E^*.

According to our MC data, for the thick sample (d=50 nm), both surfaces take part in the conductance. Such situation corresponds to the band bending illustrated in Fig. 5, b, where both E^* values are above E_f. With a decrease of the film thickness, above mentioned downward shift of E_c (Fig. 5, c) results in succesively switching off the interface contribution (one of the energies E^* crosses E_f). This can explain the experimentally observed decrease of the number of conducting surface channels responsible for WAL, when the TI film thickness decreases from 50 nm to 30 nm. At a further decrease of the film thickness both E^* values could occur below E_f (Fig. 5, d), indicating the dissapearance of WAL determined by the surface channels. This is in line with the experimentally observed bulk related WL instead of WAL in MC of 20 nm sample. Thus, our qualitative picture shows the possible scenario of the surface-state contribution to the WAL depending on the TI film thickness.

In principle, the topological states of TI can co-exist with a two-dimensional electron gas (2DEG) [43], arising from the surface band-bending effect. Due to Rashba spin splitting [44], the 2DEG states could contribute to the WAL effect. However, this contribution depends on the SOI strength, expressed as spin splitting value $\Delta_r = 2\hbar\Omega$, and scattering time τ, and can be characterized by $\Omega\tau$ value [45]. With increase of the $\Omega\tau$, a crossover from weak localization to weak antilocalization can be realized (see Fig.3 in the paper [45]) at $\Omega\tau \sim 1$. We estimated the $\Omega\tau \leq 1.7$ using the mobility value ($\sim$ 700 cm^2/Vs) from our MR measurement and Rashba splitting value ($\leq$ 50 meV) from the ARPES data in the paper [44]. As a result, the zero-field correction turns out to be close to zero. Thus the contribution of 2DEG to WAL is expected to be negligible. Nevertheless, we have not enough data to absolutely exclude the contribution of 2DEG for the observed effects.

The situation becomes more complicated if we take into account possible scattering or wave functions hybridization for carriers in different channels. In this case the all characteristics will be averaged [46, 47] and parameter α_{WAL} can be close to $-1/2$. We cannot distinguish this "mixed" channel from the independent TI surface one, but in any case the TI surface states should take part in the observed experimental WAL effect.

Additional information of the charge transport behavior in TI films, as shown in [33], can be obtained from the analysis of the correction to the conductivity in a parallel field, which is described using the equation:

$$\Delta\sigma_{||}(B) = \sum_{i=1}^{2} \alpha_i \frac{e^2}{2\pi^2\hbar} \left[\ln\left(1 + \beta_i \frac{d^2 e^2 L_i^2}{\hbar^2} B^2\right)\right], \quad (3)$$

where parameters α_i and L_i are determined from the MC analysis in a perpendicular field, β_i is a parameter that depends on the transport mechanism. The line in the inset to Fig. 4 shows the approximation of the MC in a parallel field for sample 3 by equation (3), while the fit was performed with parameters $\alpha_{WAL} \sim -1$, and $L_{WAL} \sim 0.5$ μm. The resulting $\beta_{WAL} \sim 0.2$ value indicates the Beenakker-von Hauten [48] transport mode. This regime corresponds to the situation when the free path of charge carriers is comparable to the film thickness and the conduction channels are weakly coupled to each other. This result confirms the conclusion about the contribution of two independent surfaces of 3D TI to the WAL.

5. Conclusion

Large area Bi_2Se_3 films with different thickness were grown on CVD graphene by physical vapor deposition. The analysis of the conductivity and magnetoresistance shows that despite the high TI bulk conductivity, in Bi_2Se_3/graphene films it is possible to separate the contribution of two surface channels of topologically protected states. The obtained results point out the high interface boundaries quality of the Bi_2Se_3 film grown on graphene. The suppression of WAL associated with surface channels and a transition to WL was observed when the film thickness is decreased. The results were explained by the dependence of the band bending of TI/Gr and TI/air interfaces on the TI film thickness.

6. Acknowledgements

The authors thank Prof. L.E. Golub for the useful discussion. The work was supported by the grant of the Ministry of Science and High Education N 075-15-2020-797 (13.1902.21.0024).

References

[1] B. A. Bernevig and S. C. Zhang, Phys. Rev. Lett. **96**, 106802 (2006). https://doi.org/10.1103/PhysRevLett.96.106802
[2] L. Fu and C. L. Kane, Phys. Rev. B **76**, 045302 (2007). https://doi.org/10.1103/PhysRevB.76.045302
[3] V. F. Gantmakher. Electrons and Disorder in Solids, Oxford University Press, 2005. DOI: 10.1093/acprof:oso/9780198567561.001.0001
[4] Nicholas P. Breznay, Hanno Volker, Alexander Palevski, Riccardo Mazzarello, Aharon Kapitulnik, and Matthias Wuttig. Phys. Rev. B **86**, 205302 (2012). DOI: 10.1103/PhysRevB.86.205302
[5] Hai-Zhou Lu, Shun-Qing Shen, Phys. Rev. B **84**, 125138 (2011). https://doi.org/10.1103/PhysRevB.84.125138
[6] J.Wang, A. M. DaSilva, C. Z. Chang, K. He, J. K. Jain, N. Samarth, X. C.Ma, Q. K. Xue, M.H.W. Chan, Phys. Rev. B **83**, 245438 (2011). https://doi.org/10.1103/PhysRevB.83.245438
[7] J. Chen, X. Y. He, K. H.Wu, Z. Q. Ji, L. Lu, J. R. Shi, J. H. Smet, Y. Q. Li, Phys. Rev. B **83**, 241304(R) (2011). https://doi.org/10.1103/PhysRevB.83.241304
[8] J. E. Moore, Nature **464**, 194 (2010). https://doi.org/10.1038/nature08916
[9] M. Z. Hasan, C. K. Kane, Rev. Mod. Phys. **82**, 3045 (2010). DOI: 10.1103/RevModPhys.82.3045
[10] X. L. Qi, S. C. Zhang, Rev. Mod. Phys. **83**, 1057 (2011). DOI: 10.1103/RevModPhys.83.1057
[11] S. Q. Shen, Topological insulators. Springer, Berlin, (2012). ISBN: 9811046050
[12] H. L. Peng, K. J. Lai, D. S. Kong, S. Meister, Y. L. Chen, X. L. Qi, S. C. Zhang, Z. X. Shen, Y. Cui, Nat. Mater. **9**, 225 (2010). https://doi.org/10.1038/nmat2609
[13] Y. Xia, D. Qian, D. Hsieh, L. Wray, A. Pal, H. Lin, A. Bansil, D. Grauer, Y. S. Hor, R. J. Cava, M. Z. Hasan, Nat. Phys. **5**, 398 (2009). https://doi.org/10.1038/nphys1274
[14] O. E. Tereshchenko, K. A. Kokh, V. V. Atuchin, K. N. Romanyuk, S. V. Makarenko, V. A. Golyashov, A. S. Kozhukhov, I. P. Prosvirin, and A. A. Shklyaev. JETP Letters, **94** 465468 (2011). https://doi.org/10.1134/S0021364011180159

[15] Y. S. Hor et al., Phys. Rev. B **79**, 195208 (2009). https://doi.org/10.1103/PhysRevB.79.195208

[16] E. Annese, T. Okuda, E. F. Schwier, H. Iwasawa, K. Shimada, M. Natamane, M. Taniguchi, I. P. Rusinov, S. V. Eremeev, K. A. Kokh, V. A. Golyashov, O. E. Tereshchenko, E. V. Chulkov, and A. Kimura. Phys. Rev. B **97**, 205113 (2018). https://doi.org/10.1103/PhysRevB.97.205113

[17] A. M. Shikin, I. I. Klimovskikh, S. V. Eremeev, A. A. Rybkina, M. V. Rusinova, A. G. Rybkin, E. V. Zhizhin, J. Sánchez-Barriga, A. Varykhalov, I. P. Rusinov, E. V. Chulkov, K. A. Kokh, V. A. Golyashov, V. Kamyshlov, O. E. Tereshchenko. Phys Rev B **89**, 125416 (2014). https://doi.org/10.1103/PhysRevB.89.125416

[18] I.V. Zhevstovskikh, Y.S. Ponosov, S.G. Titova, N.S. Averkiev, V.V. Gudkov, M.N. Sarychev, T.V. Kuznetsova, K.A. Kokh, and O.E. Tereshchenko. Phys. Status Solidi B, **255**, 1800264 (2018). DOI: 10.1002/pssb.201800264

[19] M. Lang, L. He, X. Kou, P. Upadhyaya, Y. Fan, H. Chu, et al., Nano Lett. **13**, 48 (2013). https://doi.org/10.1021/nl303424n

[20] L. Kou, F. Hu, B. Yan, T. Wehling, C. Felser, T. Frauenheim, C. Chen, Carbon **87**, 418 (2015). doi:10.1016/j.carbon.2015.02.057

[21] L. Kou, B. Yan, F. Hu, S.-C. Wu, T. O. Wehling, C. Felser, C. Chen, T. Frauenheim, Nano Lett. **13**, 6251 (2013). https://doi.org/10.1021/nl4037214

[22] K. H. Jin, S. H. Jhi, Phys. Rev. B **87**, 075442 (2013). DOI: 10.1103/PhysRevB.87.075442

[23] Kenan Song, David Soriano, Aron W. Cummings, Roberto Robles, Pablo Ordejón, and Stephan Roche. Nano Lett. **18**, 2033 (2018). https://doi.org/10.1021/acs.nanolett.7b05482

[24] J. Chae, S-H. Kang, S.H. Park, et al., ACS Nano **13**, 3931 (2019). https://doi.org/10.1021/acsnano.8b07012

[25] J. Zhang, C. Triola, E. Rossi, Phys. Rev. Lett. **112**, 096802 (2014). https://doi.org/10.1103/PhysRevLett.112.096802

[26] Dmitrii Khokhriakov, Anamul Md. Hoque, Bogdan Karpiak, Saroj P. Dash. Nat Commun **11**, 3657 (2020). https://doi.org/10.1038/s41467-020-17481-1

[27] Zhang, L., Yan, Y., Wu, H.-C., Yu, D., Liao, Z.-M.. ACS Nano, **10**, 3816 (2016). https://doi.org/10.1021/acsnano.6b00659

[28] Wenhui Dang, Hailin Peng, Hui Li, Pu Wang, and Zhongfan Liu. Nano Lett. **10**, 2870 (2010). https://doi.org/10.1021/nl100938e

[29] I. V. Antonova, N. A. Nebogatikova, N. P. Stepina, V. A. Volodin, V. V. Kirienko, M. G. Rybin, E. D. Obrazstova, V. A. Golyashov, K. A. Kokh, and O. E. Tereshchenko. J Mater Sci **56** 9330 (2021). https://doi.org/10.1007/s10853-021-05836-y

[30] S. Hikami, A. Larkin, Y. Nagaoka, Prog. Theor. Phys. **63**, 707 (1980). DOI: 10.1143/PTP.63.707

[31] J. L. Olsen, Electron Transport in Metals (Interscience, New York, 1962).

[32] J. M. Ziman, Electrons and Phonons: The Theory of Transport Phenomena in Solids (Clarendon Press, Oxford), p. 504 (1960). DOI:10.1093/acprof:oso/9780198507796.001.0001

[33] C. J. Lin, X. Y. He, J. Liao, X. X. Wang, V. Sacksteder IV, W. M. Yang, et al. Phys. Rev. B **88**, 041307(R) (2013). https://doi.org/10.1103/PhysRevB.88.041307

[34] H.-T. He, G. Wang, T. Zhang, I.-K. Sou, G. K. L. Wong, J.-N. Wang, H.-Z. Lu, S.-Q. Shen and F.-C. Zhang, Phys. Rev. Lett., **106**, 166805 (2011). https://doi.org/10.1103/PhysRevLett.106.166805

[35] Namdong Kim, Paengro Lee, Youngwook Kim, Jun Sung Kim, Yongsam Kim, Do Young Noh, Seong Uk Yu, Jinwook Chung, and Kwang S. Kim. ACS Nano **8**, 1154 (2014). https://doi.org/10.1021/nn405503k

[36] M. Liu, J. Zhang, C. Z. Chang, Z. Zhang, X. Feng, K. Li, K. He, L. Wang, X. Chen, X. Dai, Z. Fang, Q. K. Xue, X. Ma, Y. Wang, Phys. Rev. Lett. **108**, 036805 (2012). https://doi.org/10.1103/PhysRevLett.108.036805

[37] D. Zhang, A. Richardella, D. W. Rench, S. Y. Xu, A. Kandala, T. C. Flanagan, H. Beidenkopf, A. L. Yeats, B. B. Buckley, P. V. Klimov, D. D. Awschalom, A. Yazdani, P. Schiker, M. Z. Hasan, N. Samarth, Phys. Rev. B **86**, 205127 (2012). https://doi.org/10.1103/PhysRevB.86.205127

[38] Y. L. Chen, J. H. Chu, J. G. Analytis, Z. K. Liu, K. Igarashi, H. Kuo, X. L Qi, S. K. Mo, R. G. Moore, D. H. Lu, M. Hashimoto, T. Sasagawa, S. C. Zhang, I.R. Fisher, Z. Hussain, Z. X. Shen, Science **329**, 659 (2010). DOI: 10.1126/science.1189924

[39] L. A. Wray, S. Y. Xu, Y. Q. Xia, D. Hsieh, A. V. Fedorov, Y. S. Hor, R. J. Cava, A. Bansil, H. Lin, M. Z. Hasan, Nature Phys. **7**, 32 (2011). https://doi.org/10.1038/nphys1838

[40] A.M. Shikin, D.A. Estyunin, Yu.I. Surnin, A.V. Koroleva, E.V. Shevchenko, K.A. Kokh, O.E. Tereshchenko, S. Kumar, E.F. Schwier, K. Shimada, T. Yoshikawa, Y. Saitoh, Y. Takeda, A. Kimura. Scientific Reports **9**, 4813 (2019). https://doi.org/10.1038/s41598-019-41137-w

[41] I.I. Klimovskikh, M.M. Otrokov, D. Estyunin, S.V. Eremeev, S.O. Filnov, A. Koroleva, E. Shevchenko, V. Voroshnin, A.G. Rybkin, I.P. Rusinov, M. Blanco-Rey, M. Hoffmann, Z.S. Aliev, M.B. Babanly, I.R. Amiraslanov, N.A. Abdullayev, V.N. Zverev, A. Kimura, O.E. Tereshchenko, K.A. Kokh, L. Petaccia, G. Di Santo, A. Ernst, P.M. Echenique, N.T. Mamedov, A.M. Shikin and E.V. Chulkov. npj Quantum Materials **5**, 54 (2020). https://doi.org/10.1038/s41535-020-00255-9

[42] Hai-Zhou Lu, Junren Shi, and Shun-Qing Shen. Phys. Rev. Lett. **107**, 076801 (2011). https://doi.org/10.1103/PhysRevLett.107.076801

[43] Marco Bianchi, Dandan Guan, Shining Bao, Jianli Mi,Bo Brummerstedt Iversen, Philip D.C. King, Philip Hofmann. Nat Commun **1**, 128 (2010). https://doi.org/10.1038/ncomms1131

[44] P. D. C. King, R. C. Hatch, M. Bianchi, R. Ovsyannikov, C. Lupulescu, G. Landolt, et al. Phys. Rev. Lett. **107** 096802 (2011). DOI: 10.1103/PhysRevLett.107.096802

[45] L. E. Golub. Phys. Rev. B **71** 235310 (2005). DOI: 10.1103/PhysRevB.71.235310

[46] J. Chen, H. J. Qin, F. Yang, J. Liu, T. Guan, F. M. Qu et.al. Phys. Rev. Lett. **105**, 176602 (2010).

[47] Jifa Tian, Cuizu Chang, Helin Cao, Ke He, Xucun Ma, Qikun Xue, Yong P. Chen. Scientific reports **4**, 4859 (2014). DOI: 10.1038/srep04859

[48] C. W. J. Beenakker and H. van Houten, Phys. Rev. B **38**, 3232 (1988). https://doi.org/10.1103/PhysRevB.38.3232

Highlights

- Despite the high bulk conductivity of Bi_2Se_3 film grown on graphene, the surface states reveal itself in the weak antilocalization localization effect.
- The suppression of weak antilocalization associated with the surface channels was observed when the film thickness is decreased.
- Film thickness dependence of the magnetoresistance behavior is explained by the increasing of the band bending on both film interfaces with decrease of the film thickness.

Declaration of interests

☒ The authors declare that they have no known competing financial interests or personal relationships that could have appeared to influence the work reported in this paper.

☐ The authors declare the following financial interests/personal relationships which may be considered as potential competing interests: